DEVELOPMENT OF A PHOTOVOLTAIC INTEGRATED INSULATED CONCRETE SANDWICH PANEL

Mostafa Yossef, An Chen and Austin Downey

Synopsis: Insulated concrete sandwich panels are composed of two concrete wythes separated by an insulation layer and connected by shear connectors. This paper develops a multifunctional photovoltaic (PV) integrated insulated concrete sandwich (PVICS) panel, which can act as a passive energy system through the insulation layer and an active energy system by harvesting the solar energy using attached thin-film solar cells. The panel features an innovative co-curing scheme, where solar cells, Fiber-Reinforced Polymer (FRP) shell, and polymer concrete are manufactured together to act as a formwork for the sandwich panel. The objective of this paper is to prove the concept of PVICS based on bending test, Finite Element (FE) analysis and analytical study. It can be concluded that the test results correlate well with those from the FE and analytical models. FRP shell can act as both shear connectors and reinforcement. The panel achieved 82% Degree of Composite Action, which can provide enough strength and stiffness. Solar cells worked properly under service load. Shear-lag effect was observed for the strains along the width of the panel.

Keywords: Photovoltaic (PV) integrated insulated concrete sandwich (PVICS) panel; experimental investigation; Finite Element model; analytical solution.

ACI member **Mostafa Yossef** is an Assistant Professor at the Department of Construction and Building Engineering at Arab Academy for Science and Technology and Maritime Transport, Cairo, Egypt. He earned his PhD at Iowa State University in 2017. His research interests include energy-efficient structures, design and testing of composite material including steel, concrete and FRP. He is a licensed Engineer in Egypt.

ACI member **An Chen** is an Assistant Professor at the Department of Civil, Environmental, and Construction Engineering, Iowa State University, Ames, IA, USA. Chen has more than 4 years' experience in designing buildings. His research interests includes energy-efficient structures, recycled material utilization, bridge rehabilitation with advanced materials FRP bridge deck, solid mechanics. He is a Professional Engineer and a Leadership in Energy and Environmental Design Accredited Professional (LEED AP).

Austin R.J. Downey is a Ph.D. student and IGERT fellow in Iowa State University's Wind Energy Science, Engineering, and Policy program (WESEP). He received his B.S. from Iowa State University in Civil Engineering in 2014. His area of interest is in structural health monitoring of turbine blades and components in real time, practically in remote and extreme locations.

INTRODUCTION

Insulated concrete sandwich panels can provide a fast construction solution; act as a passive energy system to reduce heating and cooling costs; and reduce the concrete material, which results in reduced cost, weight, CO_2 emission and structural footprint. They are typically composed of two concrete wythes separated by a layer of foam insulation, which can be used as both walls (Einea et al., 1991, Einea et al., 1994; Frankl et al., 2011) and roofs (Benayoune et al., 2008; Bush and Wu, 1998; Chen et al., 2015). The two concrete wythes are connected with shear connectors, including steel wires, steel ties, solid concrete zones, etc. Recently, steel shear connectors are being replaced by Fiber-Reinforced Polymers (FRP) shear connectors, since FRP has a higher weight-to-strength ratio, non-corrosive property and more importantly, it reduces the thermal bridging between the two wythes.

Active solar energy system has been increasingly used. The Solar Investment Tax Credit (ITC) has successfully pushed hardware prices down and installer experience up. For example, the cost of solar electricity has decreased from $7.24/W in 2010 to $2.80/W in 2017 for residential applications (inflation adjusted), mostly due to the cost reduction of the photovoltaic (PV) module, which was $2.26/W in 2010 and is $0.31/W in 2017 (Fu et al., 2017). Although the price of the module will continue to decrease, there is little room for substantial reduction. Therefore, more efficient ways are required to optimize the cost such as eliminating the mounting system and develop multifunctional PV system.

To this end, this study explores the applicability of integrating PV cells with insulated concrete sandwich panels to develop a combined passive and active energy system, which can provide multifunctionality of load bearing, energy harvesting, and reducing thermal bridging to achieve a zero-carbon building system. The solar cells are attached to concrete through FRP material using a co-curing process, where the solar cells are bonded to the FRP during its curing. Polymer concrete is applied to the inner surface of the FRP shell to enhance the bond between the FRP and concrete. The co-curing effect can ensure the bond between solar cells and concrete and eliminate the need of the mounting system for the solar cells. Moreover, the FRP can be used as formwork for concrete which will speed the construction process and provide confining effect to enhance the overall shear transfer mechanism (Norris and Chen, 2016).

To prove this concept, a PV integrated concrete sandwich panel (PVICS) was manufactured and subjected to a three-point bending test in this study. The performance of solar cells was captured through J-V curves at different strains. The test data are further used to correlate with those from Finite Element (FE) and analytical models.

EXPERIMENTAL PROGRAM

The purpose of this section is to investigate the performance of a full-scale PVICS panel under three-point bending. The panel consisted of two outer concrete wythes and an inner layer of foam insulation, which was confined by the FRP shell. The solar cells were integrated to the top of the panel.

Material properties

The materials used to manufacture the panel were solar cells, FRP, concrete, steel rebars and expanded polystyrene (EPS) foam. The mean compressive strength of concrete was 3213 psi (22.15 MPa) with a standard deviation of 938 psi (6.46 MPa) and 5988 psi (41.29 MPa) with a standard deviation of 248 psi (1.7 MPa) when tested at 7 and 28 days, respectively. The steel rebars were ASTM A615 Grade 60 steel, with a yield strength of 60 ksi (414 MPa). Glass FRP was manufactured using chopped strand mat (CSM) and isophthalic resin. Properties of the fiberglass and resin are shown in Table 1. The amorphous silicon thin-film solar cells were 0.6 in. (1.52 cm) wide and 2.5 in. (6.35 cm) long. Their electrical properties are listed in Table 2. The foam was Type I EPS, which has a typical compressive strength of 10 psi (69 kPa).

When EPS foam and isophthalic resin are used for building applications, fire rating is a concern. Fire ratings are different for different applications, such as zero for buildings less than three stories, and two hours for high-rise buildings (Petersen, et al., 2017). Fire retardant materials, such as Alumina Trihydrate, can be added to the resin to increase the fire rating. Detailed information were provided in (Petersen, et al., 2015).

Table 1 Material properties

	Type	Tensile Strength ksi (MPa)	Tensile Modulus ksi (GPa)	Compressive Strength ksi (MPa)	Density pcf (gm/cm^3)
Resin	404 Isophthalic Resin	73 (503.3)	5279 (36.5)	12 (82.73)	68.67 (1.1)
E-Glass Fiber	Chopped Strand Mat	290 (2000)	10501 (72.4)	--	160 (2.56)

Table 2 Electrical properties

Solar Module Type	Wattage (W)	Voltage (V)	Open-Circuit Voltage (V)	Current (mA)	Short-Circuit Current (mA)
SP3-12	0.0255	3.0	4.5	8.5	10.7

Specimen fabrication

Specimen details - A 10 ft. (304.8 cm) long, 2.5 ft. (76.2 cm) wide and 10 in. (25.4 cm) thick PVICS panel with two 3 in. (7.62 cm) thick concrete wythes separated by a 4 in. (10.16 cm) EPS insulation foam was constructed, as shown in Figure 1.

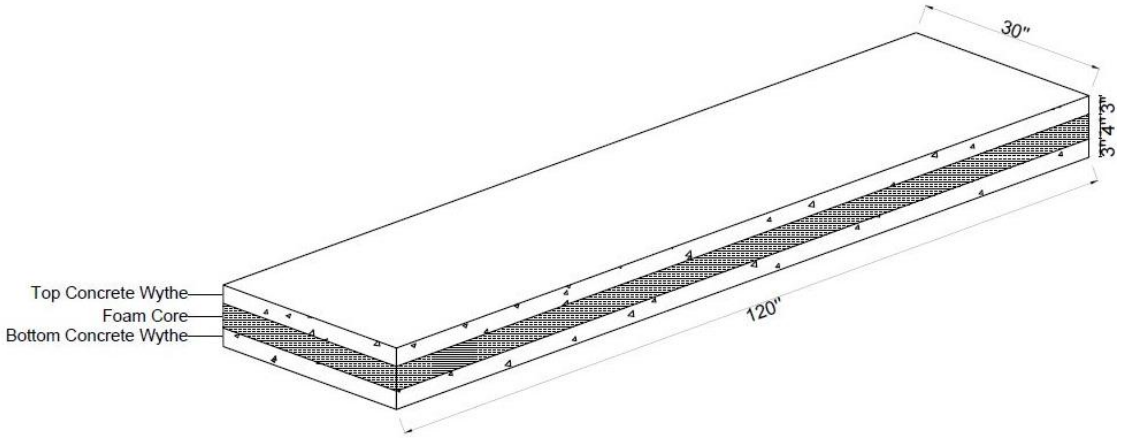

Figure 1 Typical sandwich panel (1"=2.54 cm)

Solar and FRP preparation - To manufacture the FRP with solar cells, a steel formwork with 2.5 ft (76.2 cm) wide bed was first assembled. It was then connected to the 10'' (25.4 cm) wide sides using a rubber connection in order to obtain a 90-degree angle during the folding of FRP. Four rubber connections were spaced evenly to prevent sliding of the sides while folding.

Figure 2 Attaching solar cells and laying down the glass fiber CSM

A nylon ply was laid down on the formwork to facilitate the removal of the FRP after manufacturing. They were stretched and tied to the end of each side to avoid the wrinkling of FRP. Then, eight SP3-12 thin film solar cells were attached to the nylon peel ply using 0.5 in. (1.27 cm) double sided polyimide tape to protect the solar cell area. The solar cells were placed 6 in. (15.24 cm) away from the mid-span, as shown in Figure 2. The polyimide tape was placed in the center of the solar cell, leaving 0.05 in. (0.127 cm) on both sides to be embedded in the FRP. Next, glass fiber sheet was laid down on the formwork above the solar cell, as shown in Figure 2. It is worth mentioning that the width of the panel was chosen to be 2.5 ft. (76.2 cm), as the fiberglass CSM was manufactured with a 50 in. (127 cm) width, which left the rest 20 in. (50.8 cm) to fit both sides.

Before applying the resin to fiberglass, several trials took place to develop the best practice of folding FRP. There were two major practices: the first was applying the resin on the bottom and sides, spreading the aggregates over the bottom and sides, and waiting for 45 minutes so the aggregates would attach to the sides. However, FRP buckled at the corner due to the attachment of the folding side with the formwork, as shown in Figure 3(a). The second practice was covering the corner and applying epoxy and aggregates at the sides, as shown in Figure 3(b). Then, the FRP was left for at least 1 hour until it was solidified to ensure the aggregates were well bonded. Next, the epoxy was applied to the corner and more aggregates were spread, as shown in Figure 3(c).

(a) (b) (c)

Figure 3 Different processes to fold FRP with aggregates (a) Applying epoxy and aggregates on the sides and base at the same time, (b) Applying epoxy and aggregates at the sides and base and leaving a 2'' (5.1 cm) gap at the corner, (c) Folding the sides and applying epoxy and aggregates at the corner.

The second method was chosen to manufacture the panel as the buckling effect was prevented. The same epoxy used to manufacture FRP was used to bond the aggregates. The optimum size and distribution of aggregates were chosen according to Cho et al. (2010), as shown in Table 3. Cho et al. (2010) stated that the best aggregates should be a course silica sand, known as quartzite. Due to the lack of the quartzite in Iowa, it was brought from Minnesota with 95% retained by 3/8 in. (0.95 cm) and #4-sieve analysis. Since the concrete was only at the top and lower 3 in. (7.62 cm), the aggregates were only applied to these areas, as shown in Figure 4. After the FRP had hardened, it was removed from the formwork. Oil was applied to the formwork to facilitate the removal of the FRP and panel after pouring. Before placing the steel, FRP sides were trimmed as low as 0.25 in. (0.635 cm) to provide space where the FRP can be embedded within the concrete.

Table 3 Aggregates optimum size and distribution

Optimum Size	0.157 – 0.276 in. (0.4 – 0.7 cm)
Optimum Distribution	0.82 lb./ft.^{2} (4 kg/m^2)

Figure 4 FRP-aggregate shell

Figure 5 Installing strain gages

Figure 6 Assembling rebars

Steel Reinforcement - Two sets of three steel rebars were cut and placed in each wythe. Two different sizes were chosen. No. 4 rebars with a nominal diameter of 0.5 in. (1.27 cm) were placed in the top wythe, which was close to the FRP side as it will be subjected to compression. No. 5 rebars with a nominal diameter of 5/8 in. (1.59 cm) were placed in the bottom wythe. The steel rebars were cut into 117 in (297.18 cm) pieces, allowing 1.5 in. (3.81 cm) concrete cover from each side. Each rebar was sanded at the mid-span where strain gages were installed, as shown in Figure 5.

Temperature and shrinkage No. 4 steel rebars were cut into 27 in. (68.6 cm) long and placed at a spacing required by ACI 318-14 (ACI, 2014). Figure 6 shows the assembling of the longitudinal and temperature rebars using steel ties, where 1.5 in. (3.81 cm) plastic chairs were tied to the bottom of the longitudinal rebars to provide enough clearance so that the steel would be placed on the tension side of the wythe. Steel detailing and test setup are shown in Figure 7.

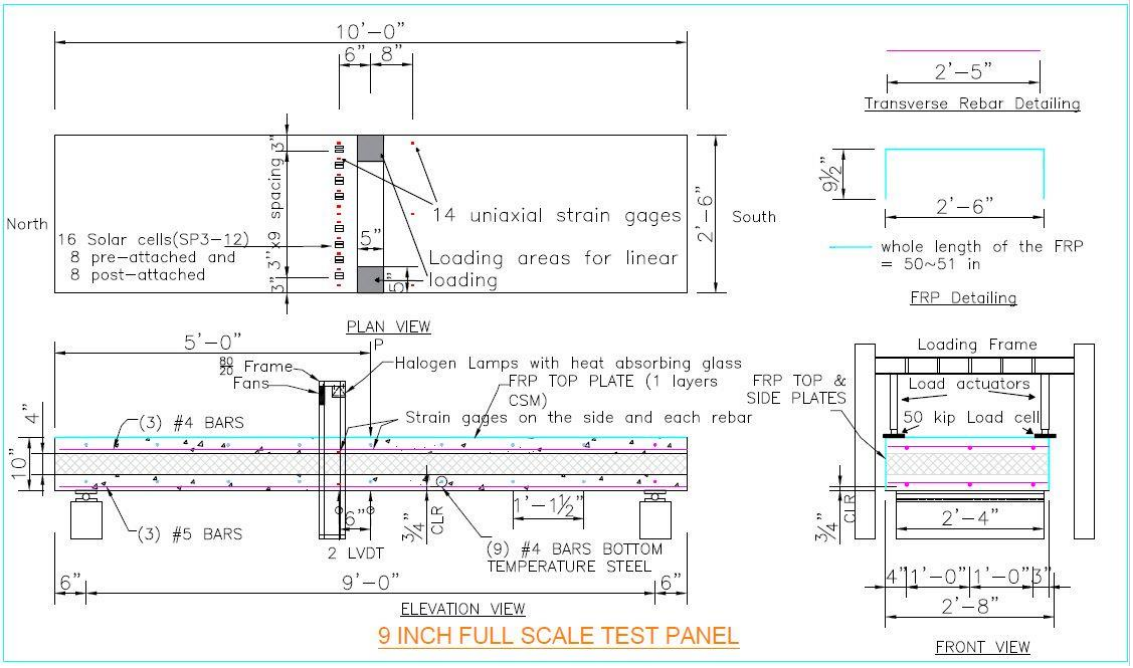

Figure 7 PVICS test setup (1"=2.54 cm; 1'=30.5 cm)

Concrete Pour - The two far ends of the formwork were closed using wood formwork. The FRP cage was coated with oil and placed in the formwork and the top steel mesh was set in plac. Four anchor bolts were installed on the two far ends near the FRP to facilitate handling and transporting of the concrete panel without subjecting it to cracking load due to its own weight.

Six concrete cylinders were poured and compacted according to ACI 318-14, where three cylinders were tested at 7 days and another three cylinders were tested at 28 days. Concrete was poured after the first set of the steel mesh was placed, where additional steel covers were installed on the top of the steel to mark the top of the concrete layer. After pouring the first layer, EPS insulation foam was placed and fitted within the panel. The second steel mesh was then placed on the top of the insulation layer. Next, the top layer of concrete was poured and leveled to provide a smooth surface for testing purpose. Figure 8(a-c) show the manufacturing process of the PVICS panel.

(a) **(b)** **(c)**

Figure 8 PVICS panel manufacturing process (a) placing first reinforcement set and pouring concrete, (b) placing insulation layer and second reinforcement set, (c) smoothing concrete surface

Test Setup

Linear stage – The concrete was cured and the formwork was removed after 28 days to ensure full strength recovery and limit any cracks that might happen due to the handling and transporting the panel. Visual inspection showed that the FRP side plates were well attached to the concrete. It was also noted that FRP was embedded inside the concrete for the most of the panel, which could improve the performance of the FRP shear connector to resist shear loads.

Test setup for the PVICS panel is shown in Figure 7 and Figure 9. Two actuators were fixed on an outer frame to subject the panel to a three-point bending load. The load was measured by two 50 kips (222.4 kN) load cells resting on 9 in. x 9 in. (22.86 cm x 22.86 cm) steel plates. These plates were resting on smaller plates of 5 in. x 5in. (12.7 cm x 12.7 cm) to simulate point loads. Two deflection transducers were installed to measure the slab at the mid-span and 6 in. (15.24 cm) away from the mid-span, respectively. Eleven Strain gages were installed along the width of the panel in between the solar cells. Another three strain gages were installed 8 in. (20.32 cm) away from the mid-span on the other side, where one strain gage was installed at the mid-width and the other at each edge. To measure the slip, two strain gages were installed at the side. The strain gages, load cells and deflection transducers were all connected to a data acquisition system where the data was synchronized and exported for analysis.

In order to validate the linear elastic analytical model, the PVICS panel was first modeled using FE model, where the cracking load was obtained. It was found that the cracking load is about 2500 lbf (11.12 kN). Therefore, the PVICS panel was loaded first under a load of 2000 lbf (8.89 kN) using a manual hydraulic jack which was connected to the two actuators as shown in Figure 9.

To investigate the performance of the solar cells, an additional frame was assembled using protruded aluminum sections to hold lamps and fans connections. Four projection halogen lamps with 150 W were installed to provide enough illumination for the 16 solar cells, where eight solar cells were installed during the manufacturing of the slab, while another eight solar cells were attached afterwards with different bonding configuration as a part of another study. Only the eight pre-attached solar cells will be discussed in this study to avoid duplication of results. Two 20 Amp Variac transformers were used to provide power for the four lamps due to the high amperage drawn by these lamps, which is eight Amps per lamp. Solar irradiance was measured using digital solar power meter which fell within the accepted range. To avoid any increase of the temperature, six fans were installed close to the lamps and held together using an aluminum plate as shown in Figure 10.

Figure 9 PVICS panel under three-point loading

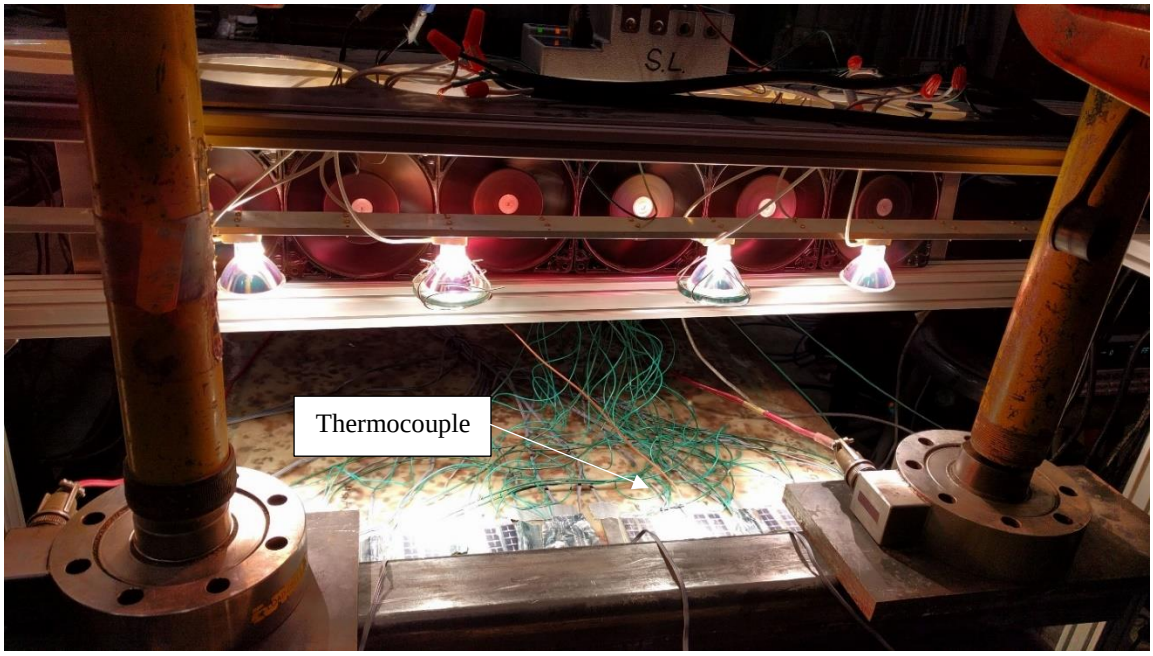

Figure 10 Nonlinear loading setup with installed lamps, fans and thermocouple

Each solar cell was connected to a terminal that was connected to a multiplexer, which was used to switch between different solar cells. The multiplexer was controlled by LabVIEW through an I/O module. Each time the multiplexer received a signal from a solar cell, it directed it to the sourcemeter. J-V curves were then measured and exported using the same LabVIEW code.

To avoid the temperature generated from the lamps, a 0.25 in. thick temperature glass was imported from the Kodak carsoul projectors and placed directly under the lamp. The temperature was measured using a thermocouple (annotated in Figure 10) placed under the second lamp. The thermocouple probe was connected to a module with 0.25˚C accuracy, which was installed in the chassis and controlled via LabVIEW code. Figure 11 shows a flow chart for the connection details for measuring multiple solar cell readings.

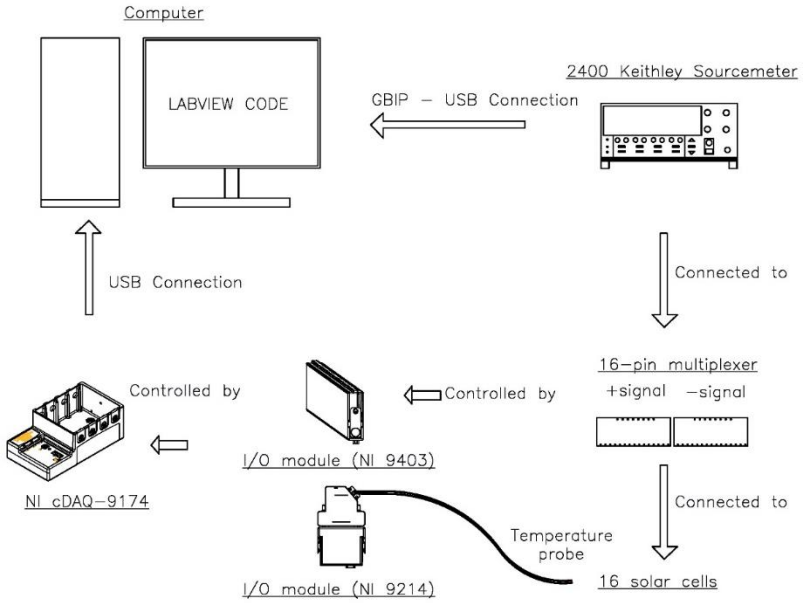

Figure 11 Multiple solar cell and temperature data acquisition setup

Recording of the results went through several steps. First, strain, deflection and load data acquisition system was turned on to start recording results. Then, initial readings were recorded for the solar cells and temperature without turning on the lights. After that, the lights were turned on and multiple readings of the temperature and solar cell readings were captured to study the behaviour of the solar cells and strain gages under temperature. After about 15 minutes, the strain gages readings were almost steady which indicates that the effect of the temperature has become stable. The strain gages, deflection transducers and load cells readings were then zeroed to compensate for the temperature effect. Incremental loading was manually applied to the panel using a hydraulic jack, where the solar cell and temperature were recorded at each increment. After the loading, the data was synchronized and analyzed, as shown in next section.

Nonlinear stage - The panel was loaded until failure to investigate the behaviour of the panel under nonlinear stage. The nonlinear setup is similar to the linear setup except for the loading part, where the two actuators were placed on the two plates. A 3 in. x 3 in. (7.62 cm x 7.62 cm) beam with box section was placed underneath the plates. In order to avoid localized effect from the steel beam, a rubber mat was cut and placed in between the FRP and steel beam, as shown Figure 10. The new setup will act as a distributed load to avoid any localized effect that could occur due to point loading.

VALIDATION AND RESULTS

Linear stage

FE validation - To validate the test results, a 3D FE model shown in Figure 12 was constructed using ABAQUS (2013). Concrete wythes and insulation foam were modeled using solid elements (C3D8R), while longitudinal and transverse rebars were modeled as truss elements (T3D2) which were embedded inside the concrete wythes. FRP plates were created as shell elements (S4R) connected to each other and other parts using tie constraint. Loads were modeled as pressure loads on two surfaces at the edge where each surface is 5 in. x 5 in. (12.7 cm x 12.7 cm) to simulate the same loading conditions in the test. The boundary conditions were set to pin and roller. The same material properties are listed in Table 4. Figure 13 and Figure 14 show close correlation between the FE and experimental results for strains and deflections in the linear region, respectively.

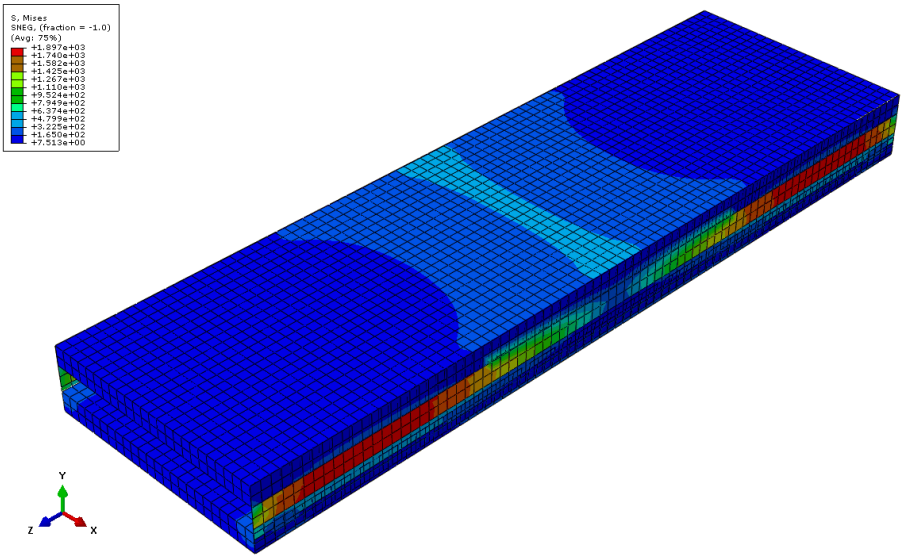

Figure 12 FE model (insulation foam is removed for clarification purpose)

Table 4 Material properties

Material	Concrete	Foam	Rebar	GFRP w Polymer aggregate
Young's Modulus ksi (GPa)	4029 (27.77)	478.6 (3.23)	29000 (200)	5000 (34.4)
Poisson's Ratio (ν)	0.15	0.35	0.3	0.2
Density pcf (gm/cm^3)	150 (2.4)	1 (0.016)	490 (7.85)	62.4 (1)

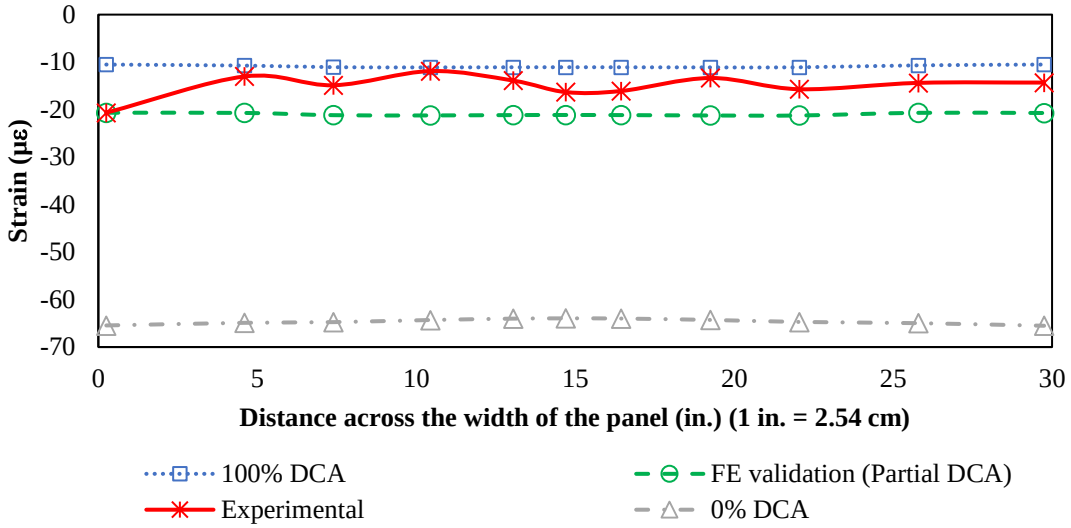

Figure 13 Correlation of strain across the width of the panel

To calculate the Degree of Composite Action (DCA) for the panel, more FE models were modeled using connector elements (CONN3D2) with moment coupling to simulate different stiffness. The connector properties were set to rigid to simulate the panel with 100% DCA while the shear stiffness was equal to zero to simulate the 0% DCA. The two results were compared with validated FE and experimental results as shown in Figure 14. The DCA based on displacement method can be calculated as:

$$DCA(100\%) = \frac{\Delta_{noncomposite} - \Delta_{partial}}{\Delta_{noncomposite} - \Delta_{composite}} \times 100 \quad (1)$$

where $\Delta_{noncomposite}$, $\Delta_{composite}$, and $\Delta_{partial}$ represent displacement at a given load corresponding to 0%, 100%, and partial DCA, respectively. Deflection was interpolated at 1000 lb. (4448.22 N) load. It can be concluded that the panel achieved an 82% DCA as shown in Table 5.

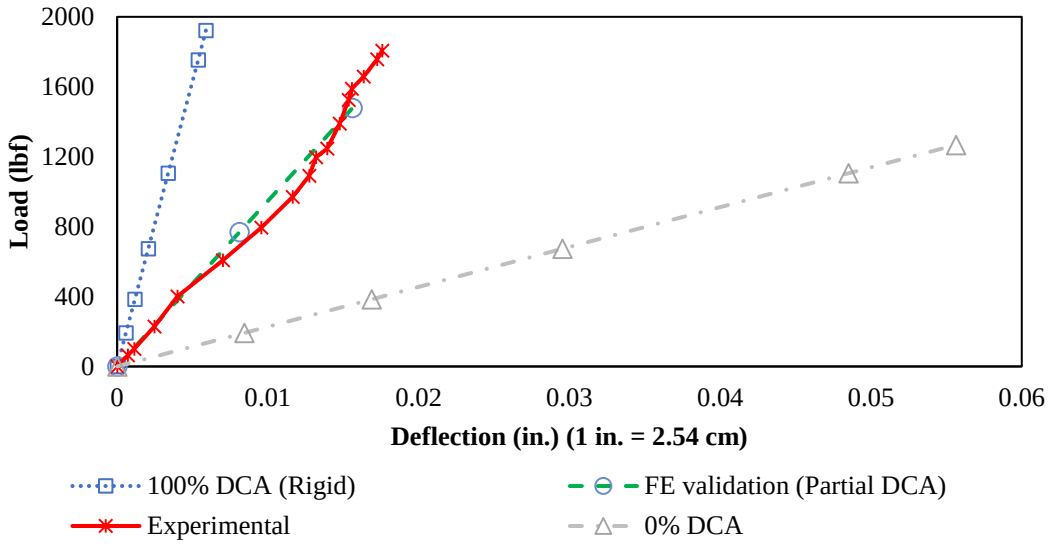

Figure 14 Correlation of mid-span deflection

Table 5 DCA calculation based on deflection method

Deflection - in. (cm)				
Load	100% DCA	Partial	0% DCA	DCA
1000	0.00306333 (0.0078)	0.01050388 (0.0267)	0.043904 (0.1115)	82%

Table 6 DCA calculation based on strain method

		0	1	2	3	5	5	7	8	9	10	x (Diff)
Strain (με)	100% DCA	10.1	9.00	6.68	5.53	2.17	-2.96	-5.83	-6.86	-8.86	-9.82	-5.14
	Partial DCA	17.2	12.4	3.07	-1.55	-15.2	13.55	0.77	-3.52	-12.3	-16.7	28.75
	0% DCA	37.0	18.4	-18.6	-37.2	-91.1	108.3	43.8	21.6	-22.7	-45.0	199.4
	DCA											86%

The DCA based on the strain method can be evaluated as:

$$DCA = 1 - \frac{x}{x_{MAX}} \tag{2}$$

where x indicates the amount of the horizontal slip which can be calculated as shown in Table 6 and Figure 15. It can be concluded that good correlation was achieved between the FE and experimental results, where DCA based on the strain method reached 86%.

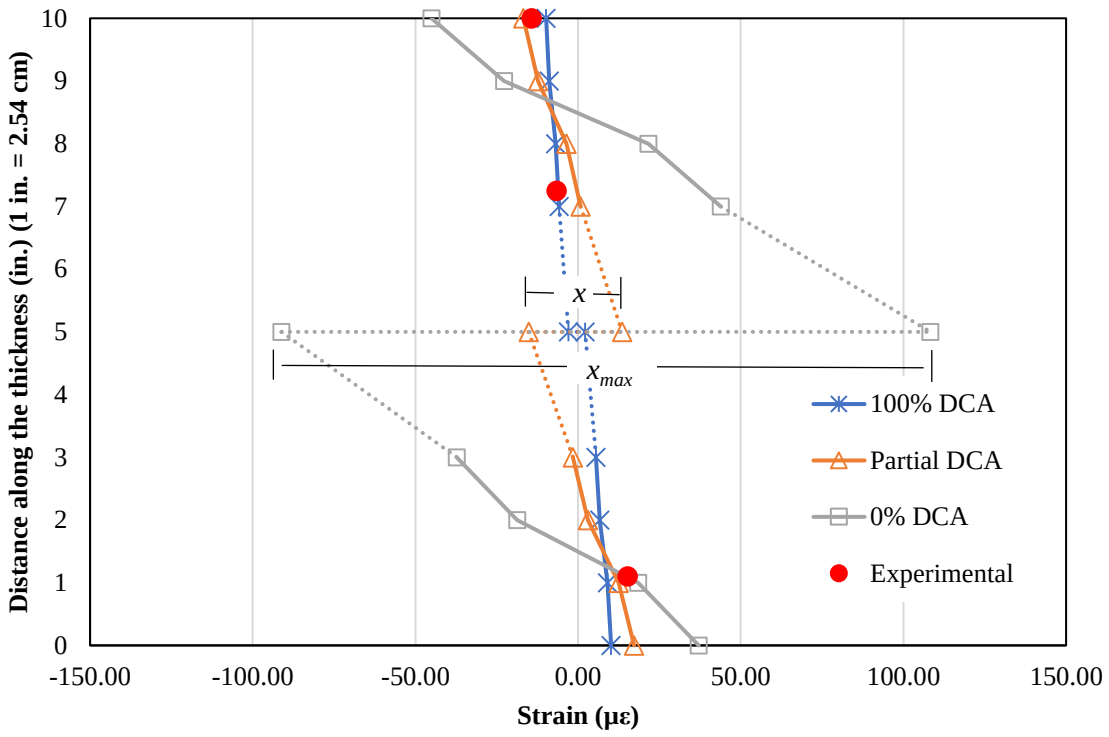

Figure 15 Strain across the thickness

Analytical model validation - An analytical model was developed by Yossef (2017) to take into consideration the effective width based on partial degree of composite action. Based on the stiffness of the panel and other geometrical and mechanical properties, DCA can be calculated as (Yossef, 2017):

$$DCA = \frac{(\alpha_{11}^{(1)} + \alpha_{11}^{(2)})N_x(x,0) - 2\dfrac{F(x)(C')^2}{b[D_{11}^{(1)} + D_{11}^{(2)}]}}{\dfrac{[M(x)](C')}{b[D_{11}^{(1)} + D_{11}^{(2)}]}} \tag{3}$$

where α_{11}, b, D_{11} and C' are geometrical properties, N_x is the stress across the wythe, $F(x)$ is the shear flow, and $M(x)$ is the moment applied to the panel, where subscripts 1 and 2 donate the upper and lower wythes, respectively. Details of these parameters can be found from Yossef (2017).

Effective width b_{eff} can then be calculated for panel with two shear connectors as:

$$b_{eff} = \frac{2 \cdot F'(x)}{N_x(x,b)} \tag{4}$$

where $F'(x)$ can be expressed as:

$$F'(x) = \sum_{j=1}^{\infty} \frac{1}{\xi_j}(C_{1j}\sinh(\xi_j b) + C_{2j}\cosh(\xi_j b))\sin(\frac{j\pi x}{a}) \tag{5}$$

The deflection $\Delta(x)$ can be calculated for a simply supported sandwich panel as:

$$\Delta(x) = (1 - DCA)\Delta_0(x) + DCA \times \Delta_{100}(x) \tag{6}$$

where Δ_0 and Δ_{100} are deflection of non-composite and full composite panels, respectively, which can be calculated as:

$$\Delta_0 = \frac{P \cdot a^3}{48 \cdot E \cdot I_{x0}}, \Delta_{100} = \frac{P \cdot a^3}{48 \cdot E \cdot I_{x100}} \tag{7}$$

where P is the applied load, a is the span, E is the equivalent Young's modulus, and I_{x0} and I_{x100} are the second moment of inertia and can be calculated as:

$$I_{x0} = 2 \cdot b\left(\frac{t^3}{12}\right), I_{x100} = 2 \cdot \left[b_{eff}\left(\frac{t^3}{12}\right) + b_{eff} \cdot t \cdot \left(\frac{C'}{2}\right)\right] \tag{8}$$

where t is the wythe thickness, b is the panel width, C' is the distance between the centerline of the upper and lower wythes. Deflection was evaluated and compared with the experimental and FE model as shown in Figure 16.

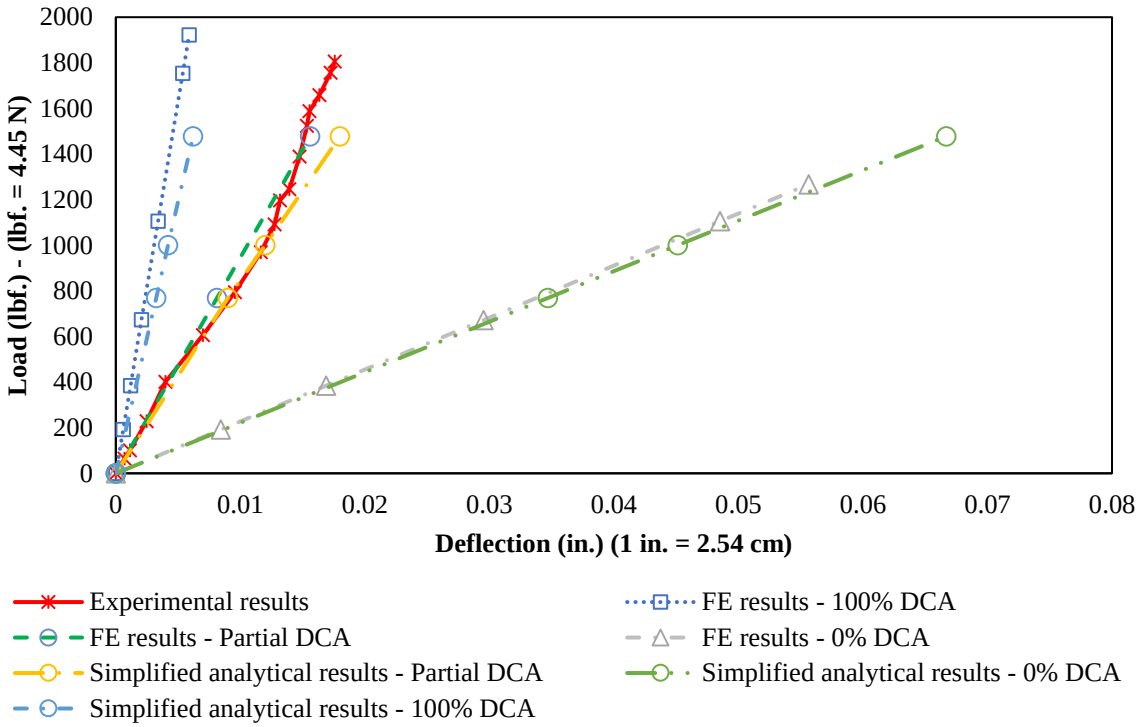

Figure 16 Validation of analytical results with experimental and FE results

Solar cell performance - The performance of the solar cells was evaluated under flexural loading, which were subjected to compression. Figure 17 shows the initial J-V curve to assess their performance before applying the load. It can be noted that the fifth solar cell is shunted or not operating which is probably due to manufacturing malfunction. Figure 18 shows a typical Maximum Power Point (MPP) and Filler Factor (FF) versus strain, where the performance of the strain remained constant. Therefore, it can be concluded that solar cells work properly under the service load.

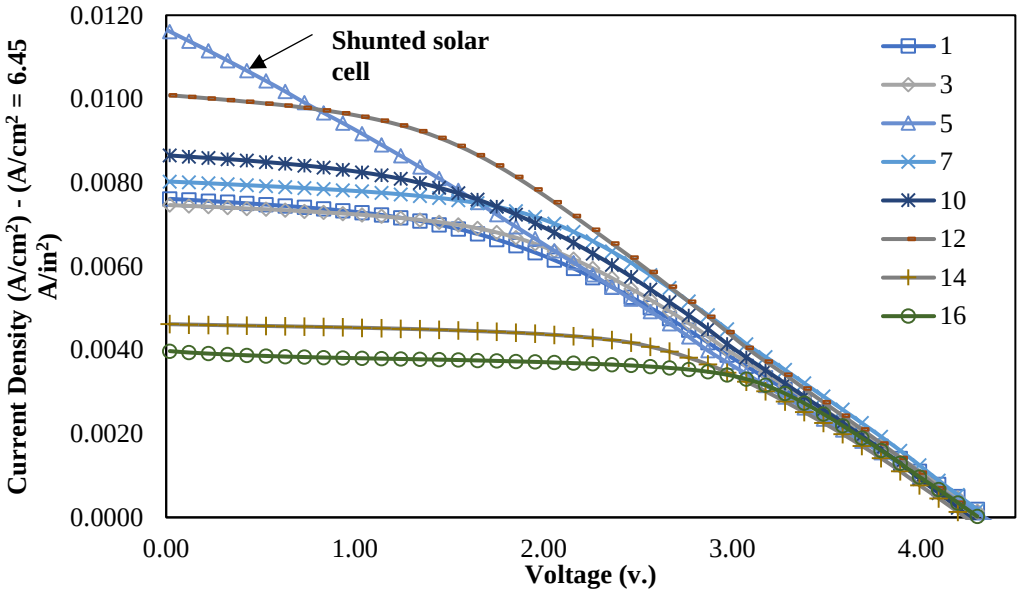

Figure 17 J-V curve before applying the load

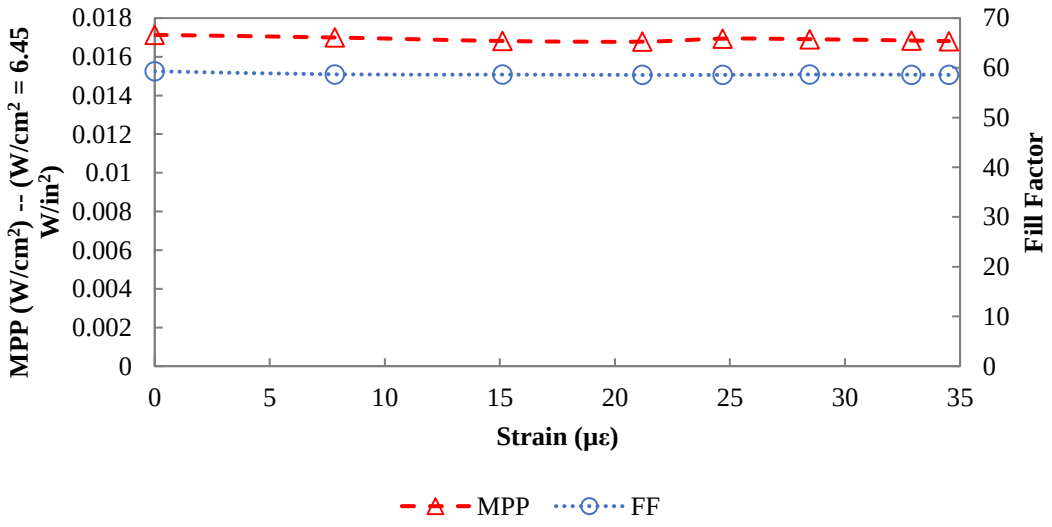

Figure 18 MPP and FF versus strain

Nonlinear stage

Structural performance - The first purpose of the nonlinear loading is to identify the full capacity of the panel. The second purpose is to investigate the behaviour of the solar cells under high strains. Figure 19 shows the load-deflection for the tested panel and FE results, where good correlation was achieved until FRP-concrete bond failure occurred. The panel was first loaded through linear range up to 4 kips (17.8 kN) where cracking sound was heard at the interface between the shear connectors and concrete. The FRP shear connectors started to buckle at the southwest side first, right above the support where the maximum shear occurred, as shown in Figure 20(a). Followed by buckling of the southeast side and then both sides started to debond until they reached near mid-span from the south side as

shown in Figure 20(b). Ultimate load was then achieved at 14.8 kips where sudden fracture of the FRP on the sides occurred as shown in Figure 20(c) and transverse crack appeared at the bottom of the panel. As the loading continued, the deflection increased rapidly and the crack width shown in Figure 21 increased. The slip between the upper and lower wythes was clearly noticed at the south side of the panel, as the north side was not affected by the loading as shown in Figure 22, which indicates that panel acts as 0% after the FRP shear connector failure. It should be noted that FE results are based on perfect bonding due to the lack of traction-separation law for FRP-concrete bond.

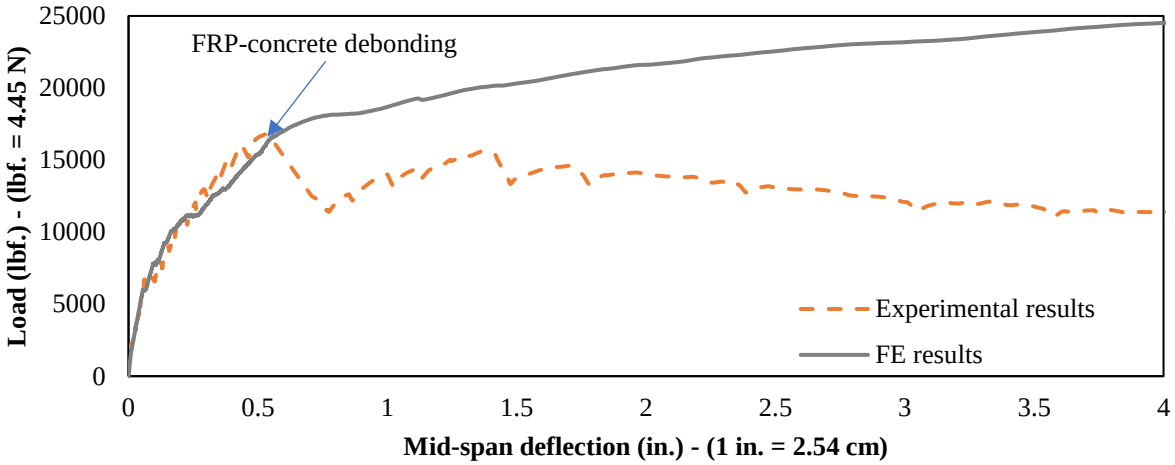

Figure 19 Load-displacement curve for experimental test and FE model

(a) (b) (c)

Figure 20 FRP shear connector failure; (a) Southwest side buckling, (b) debonding of shear connector at the southwest side, (c) Failure of shear connector at mid-span

(a) (b)

(c) (d)

Figure 21 Progress of cracks on the lower wythe

(a) (b)

Figure 22 (a) Slip at the end of the south side, (b) No slip is detected at the north side

The recorded strains at 6 in. (15 cm) north to the mid-span are plotted at different loading until failure as shown in Figure 23. The strain results illustrate the shear lag effect induced due to the shear connectors. Another strain values were recorded at 8 in. (20 cm) south to the mid-span as presented in Figure 24. Strain values were not symmetric due to localized manufacturing defect at the east side, where the FRP top plate was subjected to wrinkling effect as shown in Figure 25, which mainly happened after the FRP shear connector broke at the mid-span.

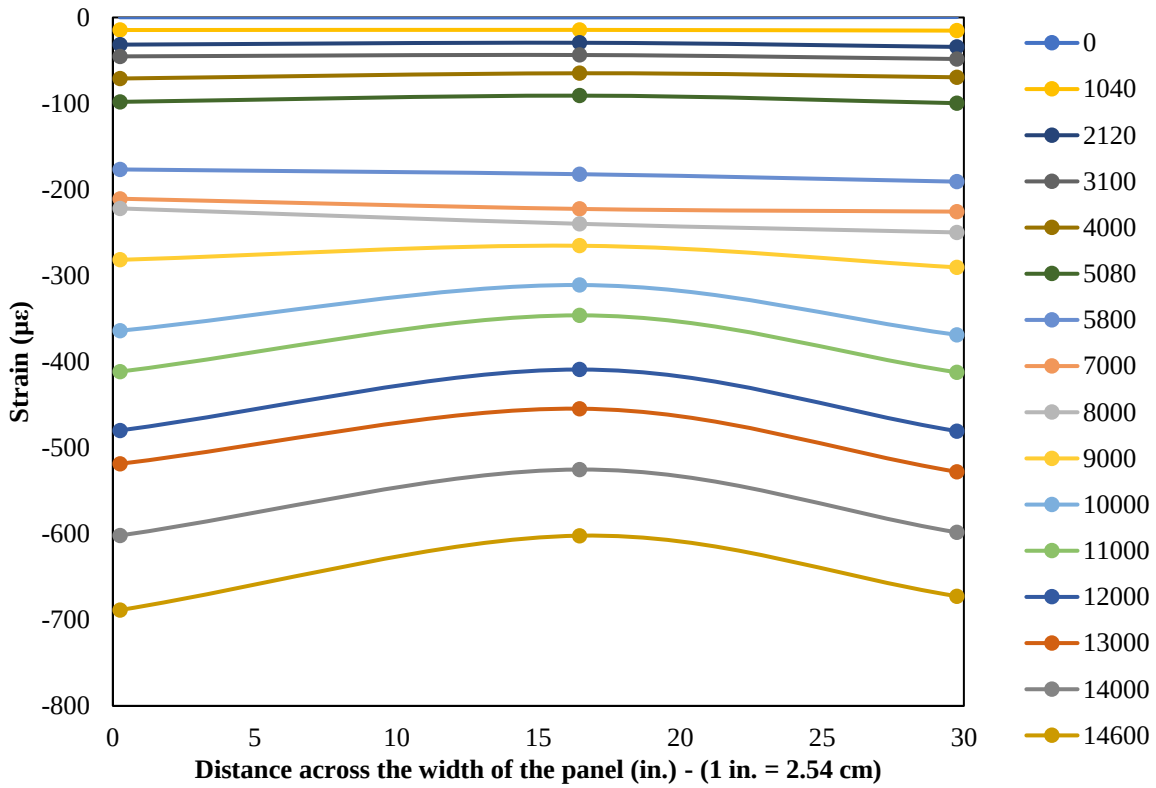

Figure 23 Strain distribution at 6 in away north mid-span at different loads

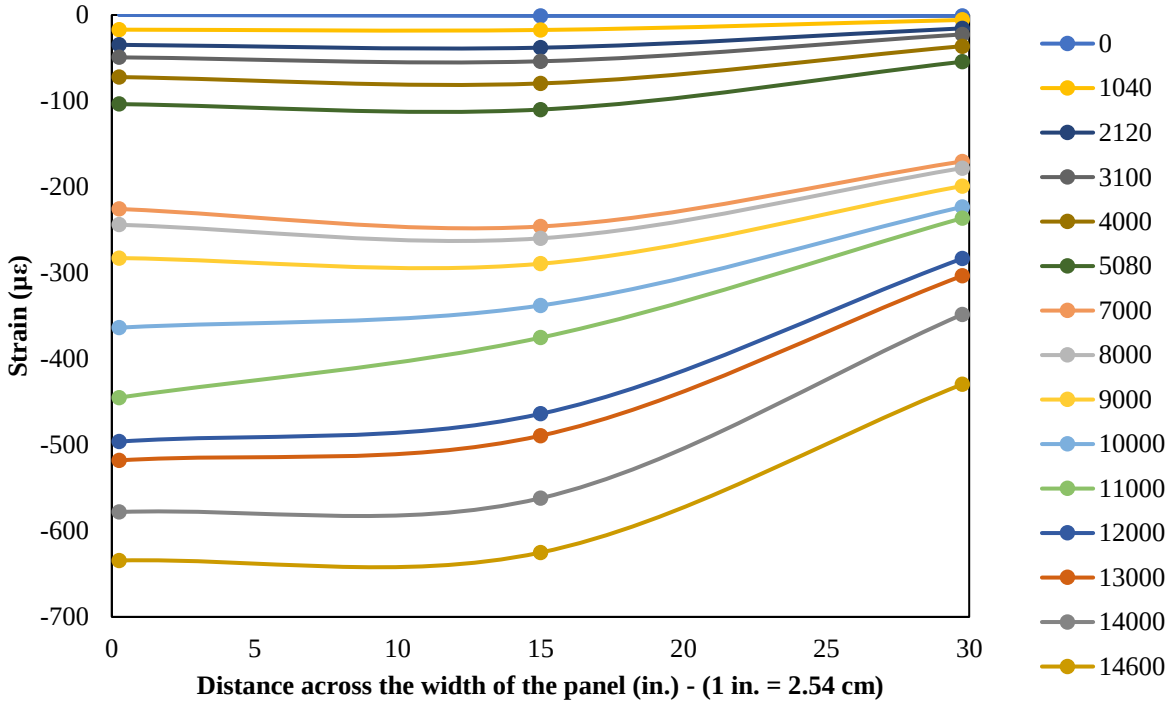

Figure 24 Strain distribution at 8 in. (20 cm) away south the mid-span at different loads

(a) (b)

Figure 25 Wrinkling of the top FRP, (a) view for east side and from the (b) west side

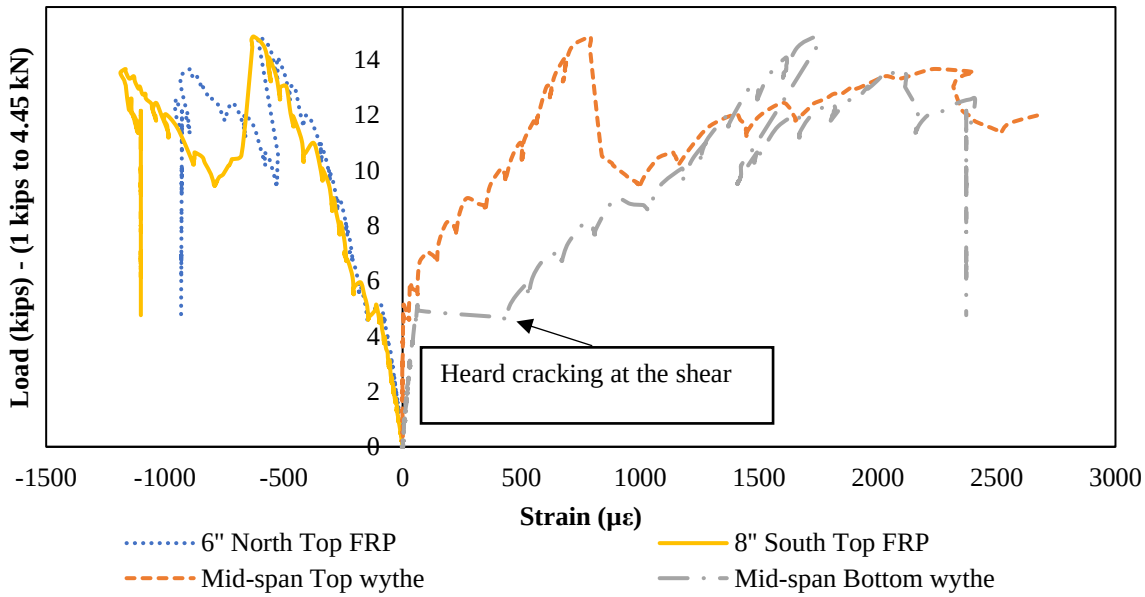

Figure 26 Strain at mid-width vs. load

Figure 26 shows the strains at the mid-width of the panel at different positions. The strain in the longitudinal rebar went through a sudden slip around 4.9 kips (21.8 kN). This happened due to cracking of the concrete under tension close to the shear connectors, which resulted in the loss of the bond between the FRP and concrete. The figure also shows that before this point, the strain in the top wythe rebar was around zero, which indicates that the panel was achieving high composite action. However, after the cracking point, the strain undergoes tension values which indicates that the panel was acting as a noncomposite or low composite action panel.

CONCLUSIONS

An innovative multifunctional sandwich panel was developed which can act as both active and passive energy system. Based on this study, several conclusions can be drawn:

1. Solar cells worked properly under the service load.
2. The panel had enough strength and stiffness, with 82% DCA.
3. The concept of PVICS was proven based on the findings from (1) and (2).
4. Shear-lag was observed for the strain across the width of the panel, which needs further investigation.
5. Further study needs to be conducted on the effect of repeated strain on the performance of solar cells, since solar cells become a part of the structure.

To fully utilize the multifunctional panel, several recommendations are provided as follows:

1. Better bond between FRP and concrete can be achieved by increasing the FRP embedded area inside the concrete from the sides.
2. To increase the strength of the shear connectors, more layers can be added or bidirectional FRP can be used at the sides.
3. As the top FRP and confinement effect can provide extra strength for the panel, top steel reinforcement can be reduced or eliminated.

ACKNOWLEDGEMENT

The authors would like to thank Douglas Wood, Owen Steffens, Ahmed Alateeq, Connor Schaeffer, David Morandeira, Hao Wu, Drs. Ashely Buss and Joseph Podolsky for their help with manufacturing the panel. The authors would also like to thank Dr. Simon Laflamme for providing equipment and for his thoughtful discussions.

REFERENCES

ABAQUS. (2013). "ABAQUS Documentation." Dassault Systèmes, Providence, RI, USA.

ACI. (2014). *Building Code Requirements for Structural Concrete (ACI 318-14) and Commentary (ACI 318R-14). ACI 318-14*.

Benayoune, A., Abdul Samad, A. A., Trikha, D. N., Abang Ali, A. A., and Ellinna, S. H. M. (2008). "Flexural behaviour of pre-cast concrete sandwich composite panel - Experimental and theoretical investigations." *Construction and Building Materials*, 22(4), 580–592.

Bush, T. D., and Wu, Z. (1998). "Flexural analysis of prestressed concrete sandwich panels with truss connectors." *PCI journal*, Precast/Prestressed Concrete Institute, 43(5), 76–86.

Chen, A., Norris, T. G., Hopkins, P. M., and Yossef, M. (2015). "Experimental investigation and finite element analysis of flexural behavior of insulated concrete sandwich panels with FRP plate shear connectors." *Engineering Structures*, 98, 95–108.

Cho, J. R., Cho, K., Park, S. Y., Kim, S. T., and Kim, B. S. (2010). "Bond characteristics of coarse sand coated interface between stay-in-place fibre-reinforced polymer formwork and concrete based on shear and tension tests." *Canadian Journal of Civil Engineering*, 37, 706–718.

Einea, A., Salmon, D. C., Fogarasi, G. J., Culp, T. D., and Tadros, M. K. (1991). "State-of-the-Art of Precast Concrete Sandwich Panels." *PCI Journal*, 36(6), 78–98.

Einea, A., Salmon, D. C., Tadros, M. K., and Culp, T. (1994). "A New Structurally and Thermally Efficient Precast Sandwich Panel System." *PCI Journal (Precast/Prestressed Concrete Institute)*, 39(4), 90–101.

Frankl, B. A., Lucier, G. W., Hassan, T. K., and Rizkalla, S. H. (2011). "Behavior of precast, prestressed concrete sandwich wall panels reinforced with CFRP shear grid." *PCI journal*, Precast/Prestressed Concrete Institute, 56(2), 42–54.

Fu, R., Feldman, D., Margolis, R., Woodhouse, M., and Ardani, K. (2017). "U.S. Solar Photovoltaic System Cost Benchmark: Q1 2017 ." National Renewable Energy Laboratory (NREL) Technical Report NREL/TP-6A20-68925. https://www.nrel.gov/docs/fy17osti/68925.pdf

Henin, E., Morcous, G.,, and Tadros, M. K. (2011). "Precast concrete sandwich panels for floor and roof applications." *PCI/NBC*, Intergovernmental Panel on Climate Change, ed., Cambridge University Press, Cambridge, 1–30.

Norris, T. G., and Chen, A. (2016). "Development of insulated FRP-confined Precast Concrete Sandwich panel with side and top confining plates and dry bond." *Composite Structures*, Elsevier Ltd, 152, 444–454.

Petersen, M.R., Chen, A., Roll, M., Jung, S.J. and Yossef, M. (2015). "Mechanical properties of fire-retardant glass fiber-reinforced polymer materials with alumina tri-hydrate filler," Composites Part B: Engineering, 78, pp. 109-121.

Petersen, M.R., Yossef, M. and Chen, A.* (2017). "Gap between Code Requirements and Current State of Research on Safety Performance of Fiber-Reinforced Polymer for Non-structural Building Components," Practice Periodical on Structural Design and Construction, ASCE, 22(4).

Sugar, J. G. (2007). "Photovoltaic Performance of Amorphous Silicon Flexible Solar Modules Under Mechanical Loading." UCLA.

Yossef, M. (2017). "Development of a multifunctional photovoltaic integrated insulated concrete sandwich panel" PhD Dissertation, Iowa State University, Ames, Iowa, USA.